

Magnetized hypermassive neutron star collapse: a central engine for short gamma-ray bursts

Masaru Shibata¹, Matthew D. Duez^{2,*}, Yuk Tung Liu², Stuart L. Shapiro^{2,†} and Branson C. Stephens²

¹*Graduate School of Arts and Sciences, University of Tokyo, Komaba, Meguro, Tokyo 153-8902, Japan*

²*Department of Physics, University of Illinois at Urbana-Champaign, Urbana, IL 61801-3080*

A hypermassive neutron star (HMNS) is a possible transient formed after the merger of a neutron star binary. In the latest magnetohydrodynamic simulations in full general relativity, we find that a magnetized HMNS undergoes ‘delayed’ collapse to a rotating black hole (BH) as a result of angular momentum transport via magnetic braking and the magnetorotational instability. The outcome is a BH surrounded by a massive, hot torus with a collimated magnetic field. The torus accretes onto the BH at a quasi-steady accretion rate $\sim 10M_{\odot}/\text{s}$; the lifetime of the torus is ~ 10 ms. The torus has a temperature $\gtrsim 10^{12}$ K, leading to copious $(\nu\bar{\nu})$ thermal radiation. Therefore, the collapse of an HMNS is a promising scenario for generating short-duration gamma-ray bursts and an accompanying burst of gravitational waves and neutrinos.

PACS numbers: 04.25.Dm, 04.30.-w, 04.40.Dg

Gamma-ray bursts (GRBs) are transient astrophysical phenomena that emit large amounts of energy (typically 10^{51} ergs) in the gamma ray band [1]. The typical time variability is shorter than 10 ms and the duration t_{dur} is ~ 10 ms–1000 s. These facts suggest that the central engine of GRBs is a stellar-mass compact object, and that the huge energy is supplied by converting gravitational binding energy into radiation. The popular theoretical candidate for the central engine is a rotating stellar-mass black hole (BH) surrounded by a massive, hot accretion torus (see [1] and references therein).

Recent observations indicate that there are at least two classes of GRBs: short-hard GRBs (hereafter SGRBs) with $t_{\text{dur}} \sim 10$ ms–2 s and long-soft GRBs with $t_{\text{dur}} \sim 2$ –1000 s. For some long GRBs, supernovae in spiral galaxies have been observed coincidentally [2], indicating that the central engine (stellar-mass BH plus torus) for long GRBs is produced through stellar core collapse of massive stars in the star forming region of spiral galaxies. By contrast, associations between SGRBs and elliptical galaxies have been reported [3]. Since elliptical galaxies have not produced massive stars in the past $\sim 10^{10}$ yrs, SGRBs are most probably not related to supernova stellar core collapse. In addition, recent observations of the afterglow of the SGRB 050709 rule out the presence of a supernova light curve and point to a binary compact object merger as the most likely central engine [4].

The merger of binary neutron stars (BNSs) has been proposed [1, 5] as a candidate for SGRBs. According to this scenario, after the merger, a stellar-mass BH is formed with an ambient accretion torus of mass ~ 1 –10% of the total. The latest general relativistic hydrodynamic (GRHD) simulations (with no magnetic fields)

have shown that just after the merger of a BNS, either a BH or a neutron star is formed [9, 10]. A BH forms promptly if the total mass of the system, M , is larger than a critical mass M_{thr} . For mergers of nearly equal-mass BNSs (the most likely case according to the data of observed binary pulsars [11]), far less than 1% of the matter remains outside the horizon, which is unfavorable for GRBs. On the other hand, for $M < M_{\text{thr}}$, a hypermassive neutron star (HMNS) forms. Here, the mass is larger than the maximum allowed mass for rigidly rotating neutron stars with an identical equation of state (EOS). An HMNS is supported against collapse mainly by rapid and differential rotation [12]. The temperature of an HMNS is high ($T \sim 10^{11}$ K) because of the heat generated by shocks during the merger process. Although T is high enough to produce a large amount of neutrinos, neutrino-antineutrino $(\nu\bar{\nu})$ pair annihilation is unlikely to generate a GRB fireball (consisting of relativistic e^+e^- pairs and photons). This is because $\nu\bar{\nu}$ annihilation occurs primarily inside the HMNSs, and the available energy is thus transferred to baryons (see e.g., [13]). However, HMNSs are transient objects and eventually collapse to BHs, alleviating this ‘baryon loading problem.’

The value of M_{thr} depends crucially on the neutron star EOS. Recent pulsar timing observations indicate [14] the existence of a neutron star of mass $2.1 \pm 0.2M_{\odot}$ (one σ error). This measurement implies that the maximum mass of spherical neutron stars, M_{sph} , is larger than $\sim 2M_{\odot}$ and that stiff EOSs are favored. The latest GRHD simulations with stiff EOSs like the one derived in [15], in which $M_{\text{sph}} \approx 2$ – $2.2M_{\odot}$, indicate that M_{thr} is ≈ 2.7 – $2.9M_{\odot}$. Thus, an HMNS is likely to be formed after a merger of BNSs of canonical mass ≈ 2.6 – $2.8M_{\odot}$ [11] rather than a prompt collapse to a BH.

The simulations in [10] also show that the HMNS remnants are rapidly and differentially rotating and have triaxial shapes. These HMNSs are secularly unstable since magnetic fields, viscosity, and/or gravitational radiation will transport and/or dissipate angular momentum and may trigger gravitational collapse. Recent nu-

*Current address: Center for Radiophysics and Space Research, Cornell University, Ithaca, NY 14853

†Also at the Department of Astronomy and NCSA, University of Illinois at Urbana-Champaign, Urbana, IL 61801

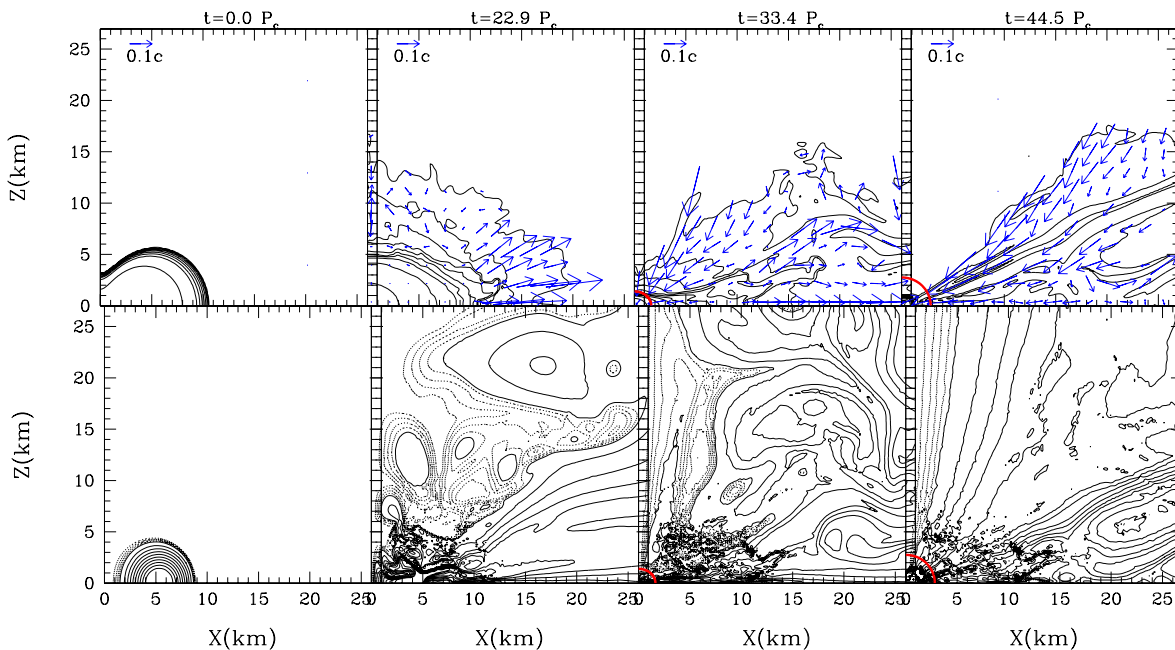


FIG. 1: Upper four panels: Snapshots of the density contours for ρ (solid curves) and velocity vectors. The contours are drawn for $\rho = 10^{15} \text{ g/cm}^3 \times 10^{-0.4i} \text{ g/cm}^3$ ($i = 0-9$). In the last panel, a curve with $\rho = 10^{11} \text{ g/cm}^3$ is also drawn. The (red) circle near the center in last two panels denotes an apparent horizon. The scale of the velocity is indicated in the upper left corner. The lower four panels denote the magnetic field (contours of the toroidal component of the vector potential A_φ) at the same times as the upper panels. The solid contour curves are drawn for $A_\varphi = 0.8(1 - 0.1i)A_{\varphi,\text{max},0}$ ($i = 0-9$) and the dotted curves are for $A_\varphi = 0.08(1 - 0.2i)A_{\varphi,\text{max},0}$ ($i = 1-4$). Here, $A_\varphi = A_{\varphi,\text{max},0}$ is the maximum value of A_φ at $t = 0$.

merical simulations [10] suggest that gravitational wave emission may trigger a collapse in $\sim 50-100$ ms for $M \gtrsim 0.9M_{\text{thr}} \sim 2.4-2.6M_\odot$ (this time scale will be longer for smaller M). In this case, the outcome will be a BH with a small disk ($\ll 0.01M_\odot$), which is not a good candidate for the central engine of SGRBs.

The other mechanisms which transport angular momentum are magnetic braking [12, 16] and the magnetorotational instability (MRI) [17, 18]. These are likely to play a crucial role when the magnetic fields in the HMNS are large enough. Magnetic braking transports angular momentum on the Alfvén time scale [12, 16], $\tau_A \sim R/v_A \sim 10^2(B/10^{15} \text{ G})^{-1} (R/15 \text{ km})^{-1/2} (M/3M_\odot)^{1/2}$ ms, where R is the radius of the HMNS. MRI occurs wherever $\partial_\varpi \Omega < 0$ [18], where Ω is the angular velocity and ϖ is the cylindrical radius. This instability grows exponentially with an e-folding time of $\tau_{\text{MRI}} = 4(\partial\Omega/\partial\ln\varpi)^{-1}$ [18], independent of the field strength. For the HMNS model considered in this paper, we find $\tau_{\text{MRI}} \sim 1$ ms. When the MRI saturates, turbulence consisting of small-scale eddies often develops, leading to angular momentum transport on a timescale likely to be much longer than τ_{MRI} [18].

To study the effect of magnetic fields, we have performed general relativistic magnetohydrodynamic (GRMHD) simulations for differentially rotating HMNSs [6] using two new GRMHD codes [7, 8]. Here, we explore HMNS collapse further by performing a simu-

lation with the following hybrid EOS: $P = P_{\text{cold}} = K_1\rho^{\Gamma_1}$ for $\rho \leq \rho_{\text{nuc}}$ and $P_{\text{cold}} = K_2\rho^{\Gamma_2}$ for $\rho \geq \rho_{\text{nuc}}$. Here, P and ρ are the pressure and rest-mass density. We set $\Gamma_1 = 1.3$, $\Gamma_2 = 2.75$, $K_1 = 5.16 \times 10^{14}$ cgs, $K_2 = K_1\rho_{\text{nuc}}^{\Gamma_1-\Gamma_2}$, and $\rho_{\text{nuc}} = 1.8 \times 10^{14} \text{ g/cm}^3$. With this EOS, the maximum gravitational mass, M (rest mass, M_b) is $2.01M_\odot$ ($2.32M_\odot$) for spherical neutron stars and $2.27M_\odot$ ($2.60M_\odot$) for rigidly rotating neutron stars. These are similar values to those in realistic stiff EOSs [15]. We construct a differentially rotating HMNS with the following characteristics: $M = 2.65M_\odot$, $M_b = 2.96M_\odot$, maximum density $\rho_{\text{max}} = 9.0 \times 10^{14} \text{ g/cm}^3$, angular momentum $J = 0.82GM^2/c$, central rotation period $P_c = 0.202$ ms, ratio of polar to equatorial radius 0.3, and rotation period at the equatorial surface $5.4P_c$. The rotation law is specified in the same way as in [6] with the differential rotation parameter $\hat{A} = 0.8$. This HMNS is similar to that found in the BNS merger simulation of [10].

For the simulation, a hybrid equation of state $P = P_{\text{cold}} + (\Gamma_{\text{th}} - 1)\rho(\varepsilon - \varepsilon_{\text{cold}})$ is used. Here, ε is the specific internal energy, and P_{cold} and $\varepsilon_{\text{cold}}$ denote the cold part of P and ε [8]. The conversion efficiency of kinetic energy to thermal energy in shocks is determined by Γ_{th} , which we set to 1.3 to conservatively account for shock heating. A seed poloidal magnetic field is added to the HMNS by specifying the φ -component of the vector potential as $A_\varphi = A_b\varpi^2\max[(P - P_{\text{cut}}), 0]$ where P_{cut} is

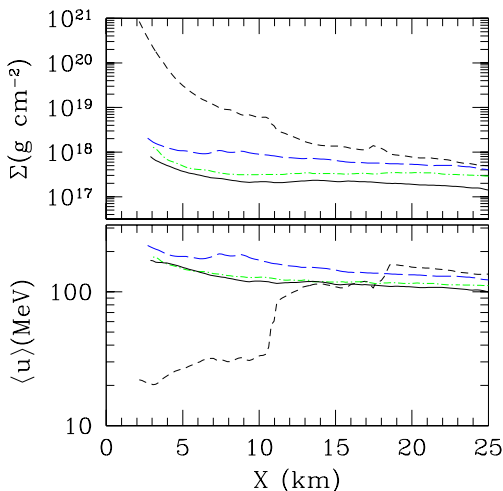


FIG. 2: Evolution of the surface density and averaged thermal energy per nucleon of the torus as functions of cylindrical radius at $t/P_c = 33.4$ (dashed curves), 39.3 (long-dashed curves), 44.5 (dotted-dashed curves), and 49.9 (solid curves).

0.04 times the maximum pressure and A_b denotes a constant which determines the initial strength of the magnetic fields. The value of A_b is chosen so that the maximum value of $C \equiv B^2/8\pi P$ at $t = 0$ is 3.42×10^{-3} . Here, $B^2/8\pi$ is the magnetic pressure. This implies that the typical magnetic field strength is $\sim 5 \times 10^{16}$ G. Such a large value is chosen to save computational time. Simulations with $1.9 \times 10^{-3} \lesssim C \lesssim 7.6 \times 10^{-3}$ indicate that a scaling relation approximately holds for smaller seed fields from $t = 0$ to BH formation via rescaling the time as t/t_A . The simulation is performed with a uniform grid of size $(N+1, N+1)$ for cylindrical coordinates (ϖ, z) , which cover the region $[0, L]$ for each direction. Here, L is chosen to be $5R$ ($R \approx 2.75M = 10.8$ km). The grid spacings are chosen as $R/100$, $R/120$, and $R/150$ ($N = 500, 600$ and 750), and approximate convergence is confirmed. Outside the HMNS, we add an atmosphere with density 10^9 g/cm³, which is necessary when employing conservative schemes for the hydrodynamic equations.

In Figure 1, we show snapshots of the meridional density contours, velocity vectors, and magnetic field lines for selected time slices. Following an initial period of linear growth ($t \lesssim t_A \approx 13P_c$), the toroidal magnetic field begins to transport angular momentum from the inner to the outer regions of the star (magnetic braking), inducing quasistationary contraction of the HMNS [6]. At $t \sim t_A$, the growth of the toroidal magnetic field saturates [16]. The subsequent evolution is dominated by MRI [18], which distorts the poloidal magnetic field lines and leads to the formation of turbulent eddies on a scale much smaller than R (see the second lower panel of Fig. 1). Because of the turbulence, the matter located near the stellar surface is blown outward. This expelled material, which is connected to the fluid in the central region, further winds up the field lines, inducing additional

magnetic braking.

The star collapses at $t \simeq 33P_c$, forming a BH composed of $\sim 85\%$ of the total rest mass (third panel of Fig. 1). Material with high enough specific angular momentum remains outside the newly formed BH and forms an accretion torus. However, the torus is secularly unstable, since magnetically-induced turbulence transports angular momentum outward. The growth of the BH by quasistationary accretion is followed by employing an excision algorithm [19]. The accretion rate \dot{M} gradually decreases and eventually settles down to $\dot{M} \sim 10M_\odot/\text{s}$. At $t \sim 50P_c$, the rest mass of the torus is $\sim 0.05M_\odot$, and the total accretion time is thus $\approx 20P_c + 0.05M_\odot/\dot{M} \sim 10$ ms. Note also that a collimated magnetic field has formed along the rotation axis (the rightmost lower panel of Fig. 1).

To clarify the properties of the torus, we calculate the surface density Σ and the vertically averaged thermal energy per nucleon, $\langle u \rangle$ (see Fig. 2). The local thermal energy per nucleon is given by $u = m_N \varepsilon_{\text{th}}$, where the thermal part of the specific internal energy is $\varepsilon_{\text{th}} \equiv \varepsilon - \varepsilon_{\text{cold}}$, and where m_N is the mass of a nucleon. (We assume that the torus is composed of free nucleons.) Thus we have

$$\Sigma(\varpi) = \int_{z \geq 0} \rho u^t \sqrt{-g} dz, \quad (1)$$

$$\langle u \rangle(\varpi) = \frac{m_N}{\Sigma(\varpi)} \int_{z \geq 0} \rho u^t \sqrt{-g} \varepsilon_{\text{th}} dz, \quad (2)$$

where g and u^t denote the determinant of the spacetime metric and the time component of the four velocity. The integrals are carried out along lines of $\varpi = \text{constant}$. Note that ε_{th} is zero at $t = 0$ inside the HMNS and subsequently grows due to shock heating. The typical thermal energy per nucleon is $u \approx 94(\varepsilon_{\text{th}}/0.1c^2)$ MeV/nucleon, or equivalently, $T \approx 1.1 \times 10^{12}(\varepsilon_{\text{th}}/0.1c^2)$ K.

Because of its high temperature and density, the torus radiates strongly in thermal neutrinos [20, 21]. However, the opacity inside the torus (considering only neutrino absorption and scattering interactions with nucleons) is $\kappa \sim 7 \times 10^{-15} T_{12}^2 \text{ cm}^2 \text{ g}^{-1}$, so that the neutrinos are effectively trapped [21]. Here, $T_{12} = T/10^{12}$ K. Since the torus is optically thick, the neutrino luminosity may be estimated in the diffusion limit [22] as $L_\nu \sim \pi R^2 F$, where R is the typical radius of the emission zone, the flux is $F \sim (c/3)(7N_\nu/4)(\sigma T^4/\tau)$ (where σ is the Stefan-Boltzmann constant and N_ν is the number of neutrino species, taken as 3), and the neutrino optical depth is $\tau \sim \kappa \Sigma$. Then $L_\nu \sim 2 \times 10^{53} \text{ erg/s} (R/10 \text{ km})^2 T_{12}^2 \Sigma_{18}^{-1}$, which is comparable to the neutrino Eddington luminosity [21]. Here, $\Sigma_{18} = \Sigma/10^{18} \text{ g cm}^{-2}$. Because of the geometry of the torus, pair annihilation will be most efficient near the z -axis. Furthermore, the surface density along the z -axis ($\varpi = 0$) outside the apparent horizon is $\Sigma_{18} \sim 0.01$ for $t \gtrsim 40P_c$, which is much smaller than the surface density of the torus. In fact, the total mass contained in a cylinder of radius $\varpi \sim M$ (~ 5 km) is $\sim 10^{-6} M_\odot$, which is likely small enough to allow the formation of a relativistic fireball [1].

Our numerical results suggest the presence of a hot, hyperaccreting torus which is optically thick to neutrinos. A model for the neutrino emission in a similar flow environment with comparable L_ν (a ‘neutrino dominated accretion flow’) is provided by Di Matteo et al. [21]. According to this model, the luminosity due to $\nu\bar{\nu}$ annihilation is $L_{\nu\bar{\nu}} \sim 10^{50}$ ergs/s [21]. Aloy et al. [23] simulate the propagation of jets powered by energy input along the rotation axis (as would be supplied by the $\nu\bar{\nu}$ annihilation). They find that if the half-opening angle of the energy injection region is moderately small ($\lesssim 45^\circ$) and the baryon density around the BH is sufficiently low, jets with the Lorentz factors in the hundreds can be produced given an energy input $L_{\nu\bar{\nu}} \gtrsim 10^{48}$ ergs/s lasting ~ 100 ms. They also show that the duration of SGRBs may be ~ 10 times longer than the duration of the energy input because of the differing propagation speeds of the jet head and tail. Our numerical results, along with the accretion flow and jet propagation models of [21, 23], thus suggest that magnetized HMNS collapse is a promising candidate for the central engine of SGRBs. Since the lifetime of the torus is ~ 10 ms in our simulation, the total energy of the $\nu\bar{\nu}$ annihilation ($E_{\nu\bar{\nu}} \sim 10^{48}$ ergs) may be sufficient to power SGRBs as long as the emission is somewhat beamed (and beaming is probably encouraged by the fat geometrical structure of the torus [23]).

Alternatively, a relativistic outflow could also be powered by MHD effects [1]. Though the GRMHD equa-

tions are solved self-consistently in our simulation, we do not find evidence for strong MHD outflows. This may be a consequence of our initial magnetic field configuration or our neglecting neutrino pressure, and requires further study. However, simulations of magnetized accretion tori in fixed Kerr spacetime [24] have found outgoing electromagnetic energy due to the Blandford-Znajek (BZ) effect [25]. The BZ luminosity [24] is estimated as $L_{\text{BZ}} \sim 10^{53} a^2 (B/10^{16} \text{ G})^2 (M/2.8M_\odot)^2$ erg/s, where a is the nondimensional BH spin parameter and B is the typical magnetic field strength. Assuming a reasonable conversion efficiency from the Poynting flux to the kinetic energy of the fireball and then to gamma-ray energy, energy fluxes of this magnitude are sufficient for forming SGRBs.

Finally, this model predicts that SGRBs should accompany a burst of gravitational radiation and neutrino emission from the HMNS delayed collapse. We plan to study this gravitational radiation in a future paper [26].

Acknowledgments: MS thanks K. Ioka and R. Takahashi for helpful comments. Numerical computations were performed on the FACOM VPP5000 at ADAC at NAOJ, on the NEC SX6 at ISAS at JAXA, and at the NCSA at UIUC. This work was supported in part by Japanese Monbukagakusho Grants (Nos. 17030004 and 17540232) and NSF Grants PHY-0205155 and PHY-0345151, NASA Grants NNG04GK54G and NNG046N90H at UIUC.

-
- [1] B. Zhang and P. Mészáros, *Int. J. Mod. Phys. A* **19**, 2385 (2004); T. Piran, *Rev. Mod. Phys.* **76**, 1143 (2005).
- [2] T. J. Galama *et al.*, *Nature*, **395**, 670 (1998); K. Z. Stanek *et al.*, *Astrophys. J. Lett.*, **591**, 17 (2003); J. Hjorth *et al.*, *Nature*, **423**, 847 (2003).
- [3] J. S. Bloom, *et al.*, astro-ph/0505480; E. Berger *et al.*, astro-ph/0508115.
- [4] D. B. Fox, *et al.*, *Nature*, **437**, 845 (2005); J. Hjorth, *et al.*, *Nature*, **437**, 859 (2005).
- [5] R. Narayan, B. Paczynski, and T. Piran, *Astrophys. J. Lett.* **395**, L83 (1992).
- [6] M. D. Duez, Y. T. Liu, S. L. Shapiro, M. Shibata, and B. C. Stephens, submitted to *Phys. Rev. Lett.*
- [7] M. D. Duez, Y. T. Liu, S. L. Shapiro, and B. C. Stephens, *Phys. Rev. D* **72**, 024028 (2005).
- [8] M. Shibata and Y.-I. Sekiguchi, *Phys. Rev. D* **72**, 044014 (2005).
- [9] M. Shibata, K. Taniguchi, and K. Uryū, *Phys. Rev. D* **68**, 084020 (2003).
- [10] M. Shibata, K. Taniguchi, and K. Uryū, *Phys. Rev. D* **71**, 084021 (2005); M. Shibata *et al.*, in preparation.
- [11] I. H. Stairs, *Science* **304**, 547 (2004).
- [12] T. W. Baumgarte, S. L. Shapiro, and M. Shibata, *Astrophys. J. Lett.* **528**, L29 (2000).
- [13] M. Ruffert and H.-T. Janka, *Astron. Astrophys.* **344**, 573 (1999).
- [14] D. J. Nice *et al.*, astro-ph/0508050.
- [15] A. Akmal, V. R. Pandharipande, and D. G. Ravenhall, *Phys. Rev. C* **58**, 1804 (1998); F. Douchin and P. Haensel, *Astron. Astrophys.* **380**, 151 (2001).
- [16] S. L. Shapiro, *Astrophys. J.* **544**, 397 (2000); J. N. Cook, S. L. Shapiro, and B. C. Stephens, *Astrophys. J.* **599**, 1272 (2003); Y. T. Liu and S. L. Shapiro, *Phys. Rev. D* **69**, 044009 (2004).
- [17] V. P. Velikhov, *Soc. Phys. JETP* **36**, 995 (1959); S. Chandrasekhar, *Proc. Natl. Acad. Sci. USA* **46**, 253 (1960).
- [18] S. A. Balbus and J. F. Hawley, *Astrophys. J.* **376**, 214 (1991); *Rev. Mod. Phys.* **70**, 1 (1998).
- [19] M. Alcubierre and B. Brügmann, *Phys. Rev. D* **63**, 104006 (2001); M. D. Duez, S. L. Shapiro, and H.-J. Yo, *Phys. Rev. D* **69**, 104016 (2004).
- [20] R. Popham, S. E. Woosley, and C. Fryer, *Astrophys. J.* **518**, 356 (1999).
- [21] Di Matteo, R. Perna, and R. Narayan, *Astrophys. J.* **579**, 706 (2002).
- [22] See, e.g., Appendix I of S. L. Shapiro and S. A. Teukolsky, *Black Holes, White Dwarfs, and Neutron Stars*, Wiley Interscience (New York, 1983).
- [23] M. A. Aloy, H.-T. Janka, and E. Müller, *Astron. Astrophys.* **436**, 273 (2005).
- [24] J. C. McKinney and C. F. Gammie, *Astrophys. J.* **611**, 977 (2004).
- [25] R. D. Blandford and R. L. Znajek, *Mon. Not. R. astr. Soc.* **179**, 433 (1977).
- [26] M. D. Duez, Y. T. Liu, S. L. Shapiro, M. Shibata, and B. C. Stephens, in preparation.